Talanta 248 (2022) 123619

Contents lists available at ScienceDirect

Talanta

journal homepage: www.elsevier.com/locate/talanta

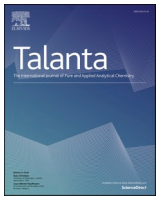

An aptamer-assisted biological nanopore biosensor for ultra-sensitive detection of ochratoxin A with a portable single-molecule measuring instrument

Tong Li, Zhuoqun Su *, Yanan Li, Lingyi Xi, Guoliang Li *

School of Food and Biological Engineering, Shaanxi University of Science and Technology, Xi'an, 710021, China

ARTICLE INFO

Keywords:
Biosensor
Nanopore
Single-molecule detection
Aptamer
Ochratoxin A

ABSTRACT

Biological nanopore-based single-molecule detection technology has shown ultrahigh sensitivity to various target analyte. But the detection scope of interesting targets is limited due to the lack of effective signal conversion strategies. In addition, conventional nanopore detection instruments are cumbersome, resulting nanopore detection can only be performed in laboratory. Herein, a customizable nanopore current amplifier is constructed to lower the cost and increase the portability of the nanopore instrument, and then an immobilized aptamer-based signal conversion strategy is proposed for α-hemolysin (α-HL) nanopore to detect small molecules (ochratoxin A, OTA). The presence of OTA in sample would trigger the release of probe single-strand DNA (ssDNA) from magnetic beads, which could subsequently cause current blockage in nanopore. The results show that the signal frequency of probe ssDNA has a linear relationship with the OTA concentration in the range of $2 \times 10^1 \sim 2 \times 10^3$ pmol/L. Compared to other methods, our sensing system has achieved an ultra-sensitive detection of OTA with the detection limit as low as 1.697 pmol/L. This strategy could broaden the scope of nanopore detection and have the potential for rapid and *in-situ* detection of other food contaminants in the future.

1. Introduction

Single-molecule detection (SMD) technologies can provide fingerprint information of a single molecule and realize the ultra-sensitive analysis of target analytes [1,2]. Such high sensitivity is essential in biological applications such as rapid detection of trace contaminants in food samples [3–5]. In particular, nanopore is a simple and label-free SMD technique, which relies on the ion current changes at pA-level when target molecules are confined in a nanometer pore across the membrane [6,7]. The current change and the blockage time reveal its identity, whereas the frequency of the blockage events reflects its concentration. In the last decades, both biological and solid-state nanopores have been widely applied in sensing of macromolecules, like DNA, RNA, PEG, peptide, and protein due to the fact that these large-size molecules can block the nanopore easily [8–10]. However, Small organic molecules are not easy to be detected directly because of their tiny size, no binding sites in the sensing area, fast dynamics, and instrument limitations.

According to the difference of pore materials, nanopore can be divided into biological and solid-state nanopore [11]. When it comes to the detection of small molecules, biological nanopores has many advantages over solid-state nanopore, e.g., smaller pore diameter (1–3 nm), accurate structure with atom precision, as well as better reproductivity [12–14]. Several strategies have been adopted to detect small molecules by biological nanopore, such as constructing binding sites in the nanopore or using macromolecules as ligand probes [15]. For example, host molecules like cyclodextrin and its derivatives are frequently used as an adaptor in α-hemolysin (α-HL) nanopore to provide a robust binding site for small guest molecules. A few guest molecules can be detected, like ATP [16], amantadine [17], glutathione [18], and so on, but the number of available guest molecules is limited. These strategies normally have a high requirement for sample purity [19], while complex matrixes in real samples would cause severe interference to the current signal. Researchers have designed some target capture probes like nucleic acid strand or ligands to enhance the target selectivity [20–22]. Although these strategies can realize the target detection in serum sample, the much more complicated matrix in food may still challenge the detection accuracy of nanopore technique. Furthermore,

* Corresponding authors.
E-mail addresses: zhuoqunsu@sust.edu.cn (Z. Su), 61254368@163.com (G. Li).

https://doi.org/10.1016/j.talanta.2022.123619
Received 25 January 2022; Received in revised form 6 May 2022; Accepted 25 May 2022
Available online 27 May 2022

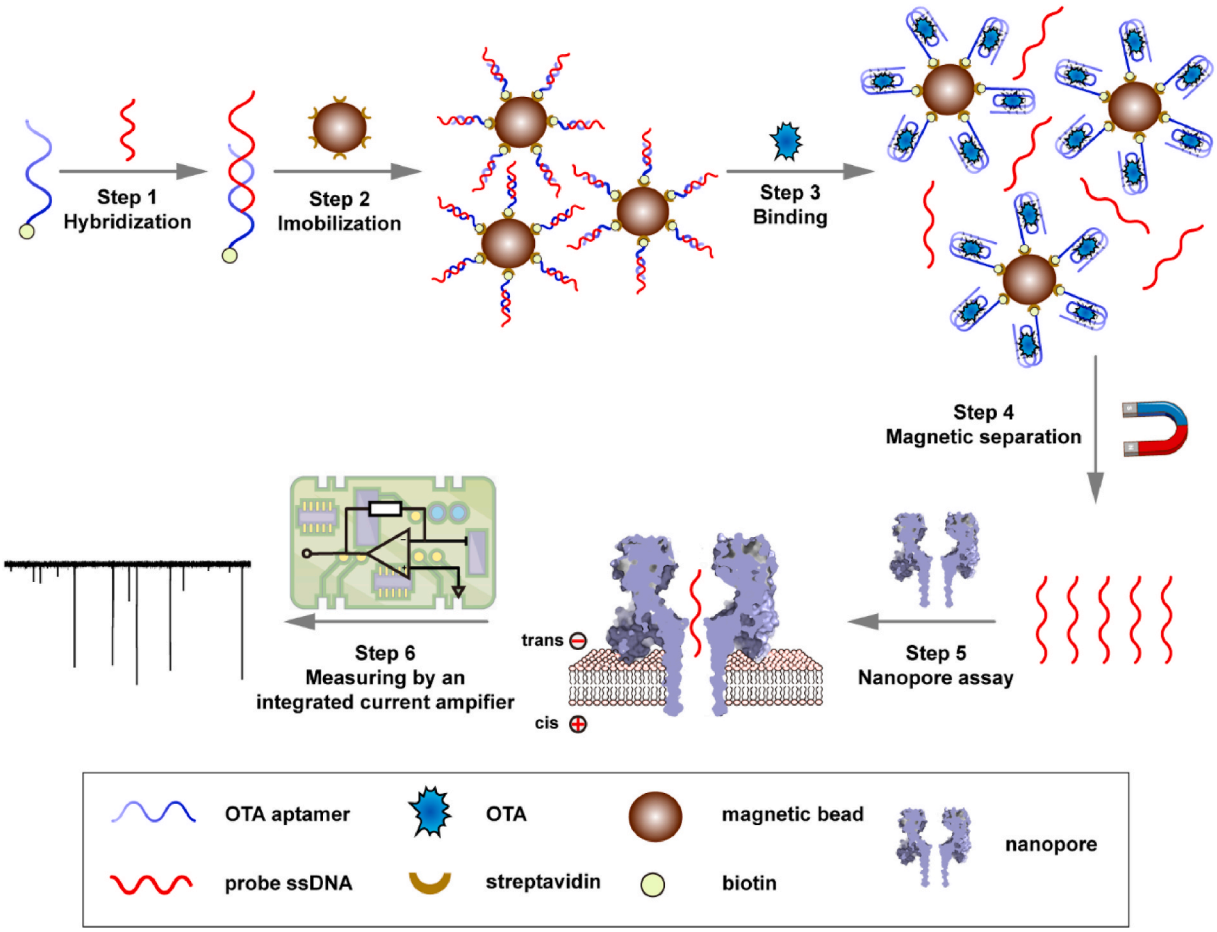

Scheme 1. Scheme of the signal conversion strategy for small molecules (OTA) detection.

most nanopore experiments rely heavily on the cumbersome and expensive commercial instruments, limiting their application in *in-situ* detection.

In this paper, we propose an immobilized aptamer-based signal conversion strategy to detect small molecules (ochratoxin A, OTA) in real sample. In specific, the presence of OTA in a sample would trigger the release of probe ssDNA from magnetic beads, which could subsequently cause current blockage in α-HL nanopore. A customizable nanopore current amplifier is constructed to lower the cost and increase the portability of nanopore instrument. This simple method can broaden the scope of nanopore detection, providing possibilities for the application of nanopores in rapid detection of other food contaminants.

2. Materials and methods

2.1. Materials and chemicals

OTA aptamer 5′-Biotin-GAT CGG GTG TGG GTG GCG TAA AGG GAG CAT CGG ACA-3′ [23], probe ssDNA without tag 5′-TGT CCG ATG C-3′, and probe ssDNA with tag poly $(dC)_{10}$ 5′-CCC CCC CCC CTG TCC GAT GC-3′ were ordered from Sangon Biotech (Shanghai). Streptavidin-coated magnetic beads were obtained from Beyotime (Shanghai). α-HL was ordered from Sigma-Aldrich (Product Number H9395). Watsons Water (Pure Distilled) was acquired from Watsons (Guangzhou). Ochratoxin A (OTA) was bought from Sopo Biological Technology (Guangzhou). Polytetrafluoroethylene film was purchased from Taobao (Shanghai, China). All the chemical reagents were of analytical grade. Corn was obtained from a local supermarket.

2.2. Single-channel current recording and data analysis

A small hole of 100 ~ 200 μm was fabricated on the polytetrafluoroethylene film (PTFE, 25 μm) by a home-made spark generator. The PTFE film with a hole was glued between the two chambers [24].

A drop of pretreated 1% hexadecane was added to each side of the film by a glass capillary tube to make the hole hydrophobic. Next, 700 μL of electrolytic buffer solution was added at both chambers, and then a drop of phospholipid (1% in hexadecane) was added to each chamber. At last, 800 μL buffer solution was added to form a phospholipid bilayer in the hole of PTFE film. The α-HL protein was added into the *trans* side where a constant voltage was applied, and the ion current was recorded by Win EDR software (V3.9.1) from Strathclyde Electrophysiology Software (Dempster, UK). The sampling rate was set to 20 kHz. DNA samples were added to the *trans* compartment. Clampfit 10.5 (Molecular Devices) was used to analyze current blockage signals, and Origin 9.0 (Microcal, Northampton, MA) was used for curve fitting and graphical representation.

2.3. Detection of OTA

100 μL streptavidin-coated magnetic beads (10 mg/mL) were taken and washed three times with 1 × TBS for magnetic separation to remove supernatant. Then, 200 μL 1 μmol/L of double-stranded DNA (dsDNA) was incubated with streptavidin-coated magnetic beads for 1 h, and the supernatant was discarded. The magnetic beads were washed three times with 1 × TBS. The volume ratio of OTA to the magnetic beads is 10:1. Different concentrations of OTA (final concentration of 2×10^1–2×10^9 pmol/L) was added to the magnetic beads and incubated at room

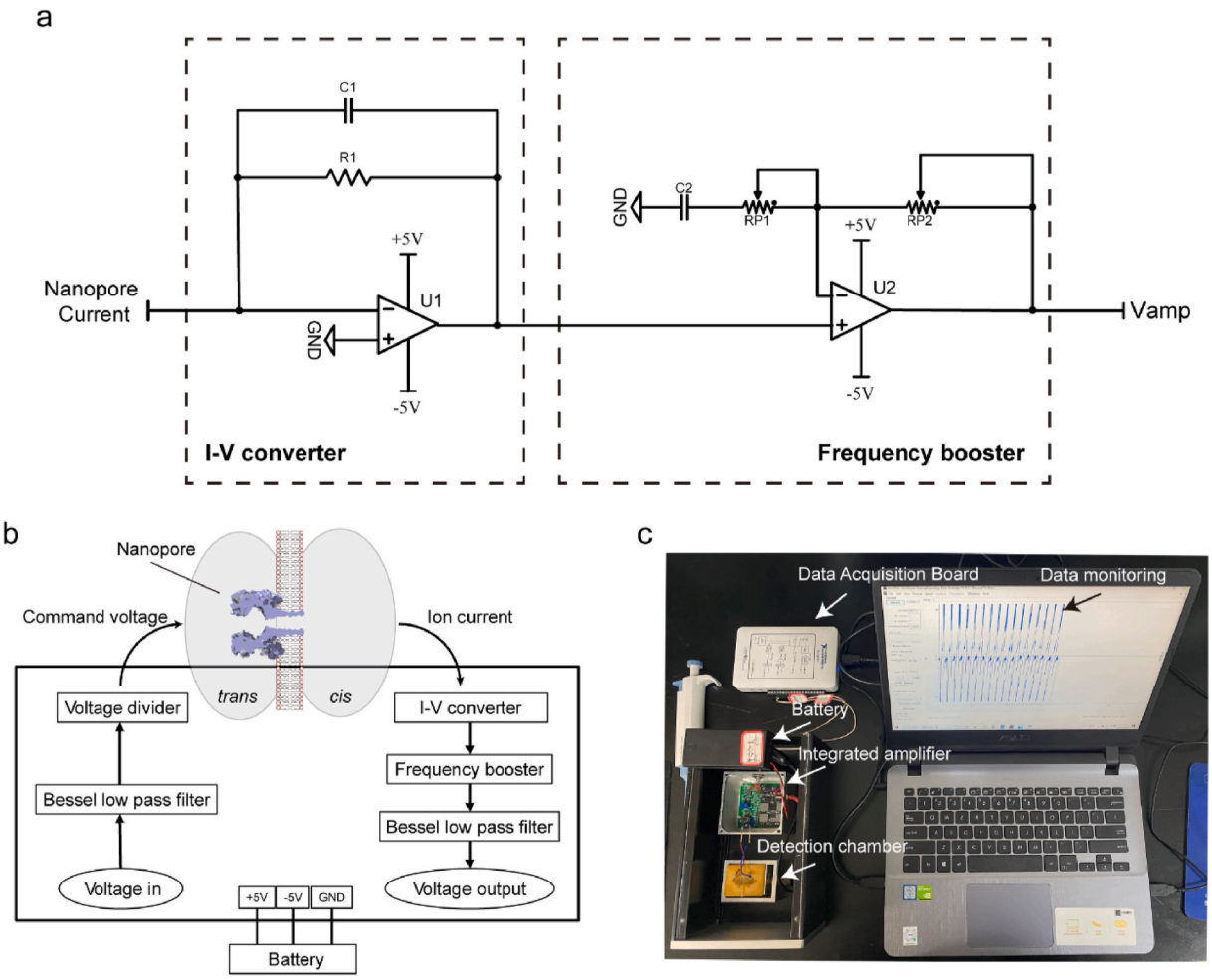

Fig. 1. Features of the customizable nanopore instrument. (a) Circuit scheme of I–V converter and frequency booster. (b) Functional block diagram of the integrated nanopore amplifier. (c) The photo of the nanopore detection system under running.

temperature for 2 h. Finally, the supernatant was added to the nanopore detection cell for the single-channel recording experiments.

3. Results and discussion

3.1. Sensing principle for OTA detection

The assay strategy is shown in Scheme 1. First, the biotinylated aptamer and the probe ssDNA were annealed together to form dsDNA. Then dsDNA with biotin in the end was immobilized onto streptavidin-coated magnetic beads via biotin-streptavidin interaction [25,26]. The beads were washed three times with 1 × TBS buffer to remove the non-specific binding fraction. The binding affinity of OTA and OTA aptamer is greater than that of probe ssDNA and OTA aptamer. OTA competes with the OTA aptamer, and binds to the action site of the OTA aptamer to form an OTA/aptamer complex, releasing the probe ssDNA dispersed to the supernatant. The supernatant was added in the *trans* chamber of nanopore system, where a command voltage was applied. With the driving force in the electric field, ions (K^+ and Cl^-) in the solution translocate through the lumen of α-HL and produce open-state current [27]. When a negatively charged probe ssDNA molecule enteres and passes through the nanopore, a transient current blockage occurs. By analyzing the frequency of blockage signals, the concentration of OTA was determined. α-HL is a stable biological nanopore and easy to obtain, so α-HL nanopore is utilized to detect probe ssDNA.

3.2. Design and assembly of nanopore current amplifier

The ion current in nanopore is generally at pA level, and the residence time of analytes is less than 1 ms [28]. To measure such weak and transient signals, we design an integrated nanopore current amplifier. The integrated nanopore current amplifier includes the following modules, i.e., command voltage modulator, current-to-voltage converter (I–V convertor), frequency booster, signal low-pass filter, and power supply module (Fig. 1a and b). The command voltage modulator process the external input voltage to reduce the noise. First, the input voltage is subjected to Bessel low-pass filtering, with amoduce cut-off frequency of 1 kHz. Then the voltage divider is utilized (division ratio: 1:20) and the smaller voltage, as a command voltage, is applied to the *trans* side of the nanopore detection chamber. To measure the nanopore current, the current-to-voltage converter, which includes an operational amplifier with low input bias current (less than 100 fA), is used. A feedback resistor of 1 GΩ is connected between the inverting input terminal and the output terminal of the operational amplifier. The pA-level current at the inverting input terminal will be converted to the voltage of mV level. At the same time, a small value capacitor (3.3 pF) is connected in parallel with the feedback resistor to stabilize the circuit and prevent oscillation (Fig. 1a). Under this condition, the theoretical bandwidth of the amplifier circuit can reach only about 5 Hz ($f = 1/2\pi RC$), which is much lower than the bandwidth required for the nanopore experiment (typically more than 1 kHz) [29]. Therefore, it is necessary to perform high-frequency compensation, and we adopt a non-inverting high-pass filter circuit (Fig. 1a), which can retain the low-frequency signal and

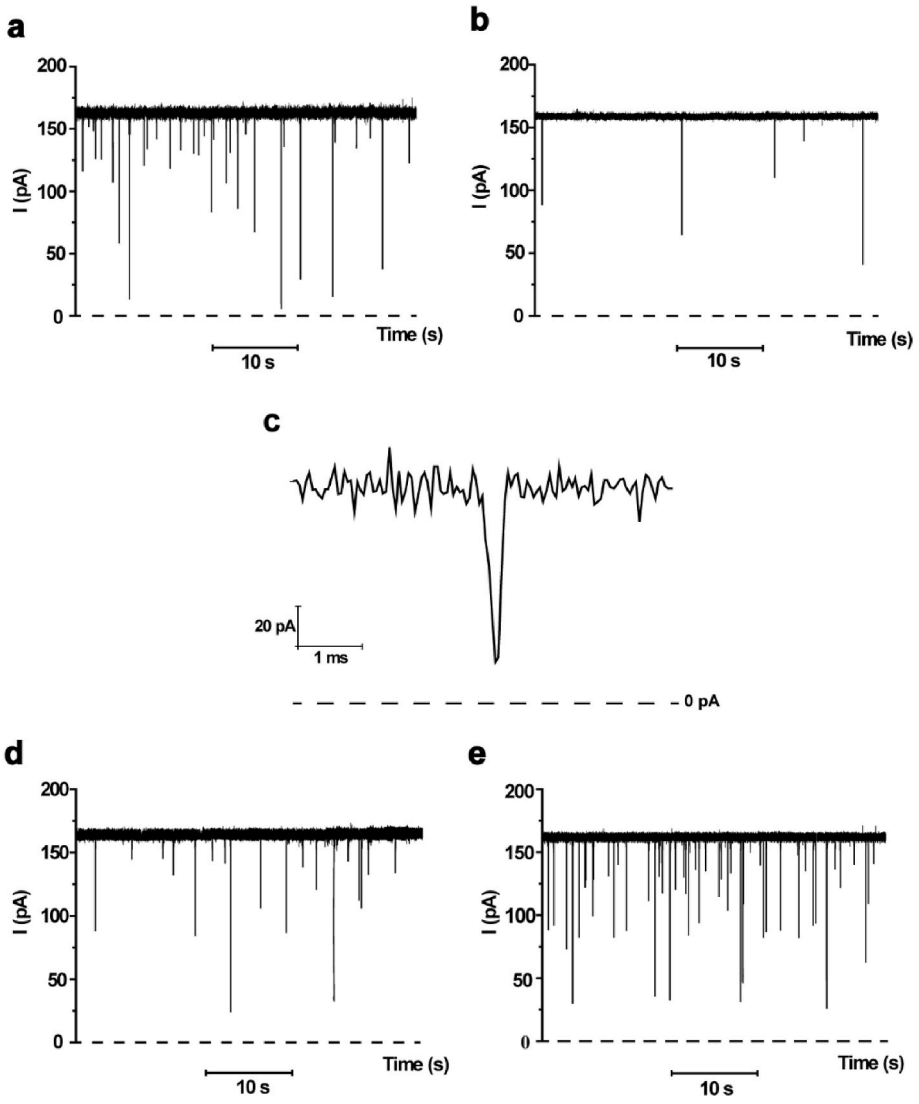

Fig. 2. The signal response of the sensing strategy in the presence (a) or absence (b) of OTA. The signal shape of probe ssDNA (c) blockage in the nanopore. The nanopore current traces for the probe ssDNA without (d), and with (e) poly $(dC)_{10}$ tag.

gain the high-frequency signal, so that the final output signal has higher bandwidth. The compensated signal is subjected to Bessel low-pass filtering with a cut-off frequency of 5 kHz to filter out high-frequency noise. The power supply module uses a lithium battery and very low-noise LDOs (low dropout regulator), which can avoid the interference of external alternating current (AC) power and increase the portability of the detection device. The integrated amplifier is connected with a data acquisition board (NI-USB 6002) and the current is recorded by the software in a laptop (Fig. 1c). We tested the performance of the nanopore current amplifier. In 1 mol/L NaCl solution, the RMS noise value of a single α-HL channel current is about 2.3 pA (Figure S1), much less than the current amplitude (about 100 pA at −100 mV). By using a standard testing module (comprised of a 1 G resistor with 100 pF capacitor in parallel), the home-made instrument shows a lower current noise compared with commercial nanopore instrument (Figure S2). Furthermore, the falling time ($t_{falling}$) of DNA blockage signal is about 80 μs, and the corresponding bandwidth is about 4.4 kHz ($0.349/t_{falling}$) [30], which is close to the cut-off frequency of low-pass filtering and can meet the requirements of single-molecule detection experiments.

3.3. Fluorescence spectrum verification

The OTA aptamer (final concentration: 1 μmol/L) labeled with the fluorophore FAM at the 3′ end was incubated with the probe ssDNA1 (final concentration: 3 μmol/L) labeled with the quenching group TAMRA at the 5′ end. The fluorescence result showed that the fluorophore FAM was quenched, indicating the hybridization between aptamer and probe ssDNA1. Then, OTA and binding buffer were added into the system. After the incubation, the fluorescence intensity increased and the fluorescence recovered (Figure S3), suggesting the strong binding between OTA and OTA aptamer.

3.4. Establishment and optimization of aptamer-assisted nanopore sensor for OTA

The hybridization and immobilization of DNA were monitored by agarose gel electrophoresis [31]. When OTA aptamer (1 μmol/L) and probe ssDNA (3 μmol/L) were annealed together, the electrophoretic mobility of DNA slowed down, indicating the formation of dsDNA (Figure S4). The dsDNA ended with biotin was added into the solution of streptavidin-coated magnetic beads. The disappearance of the dsDNA band in agarose gel electrophoresis means the success of

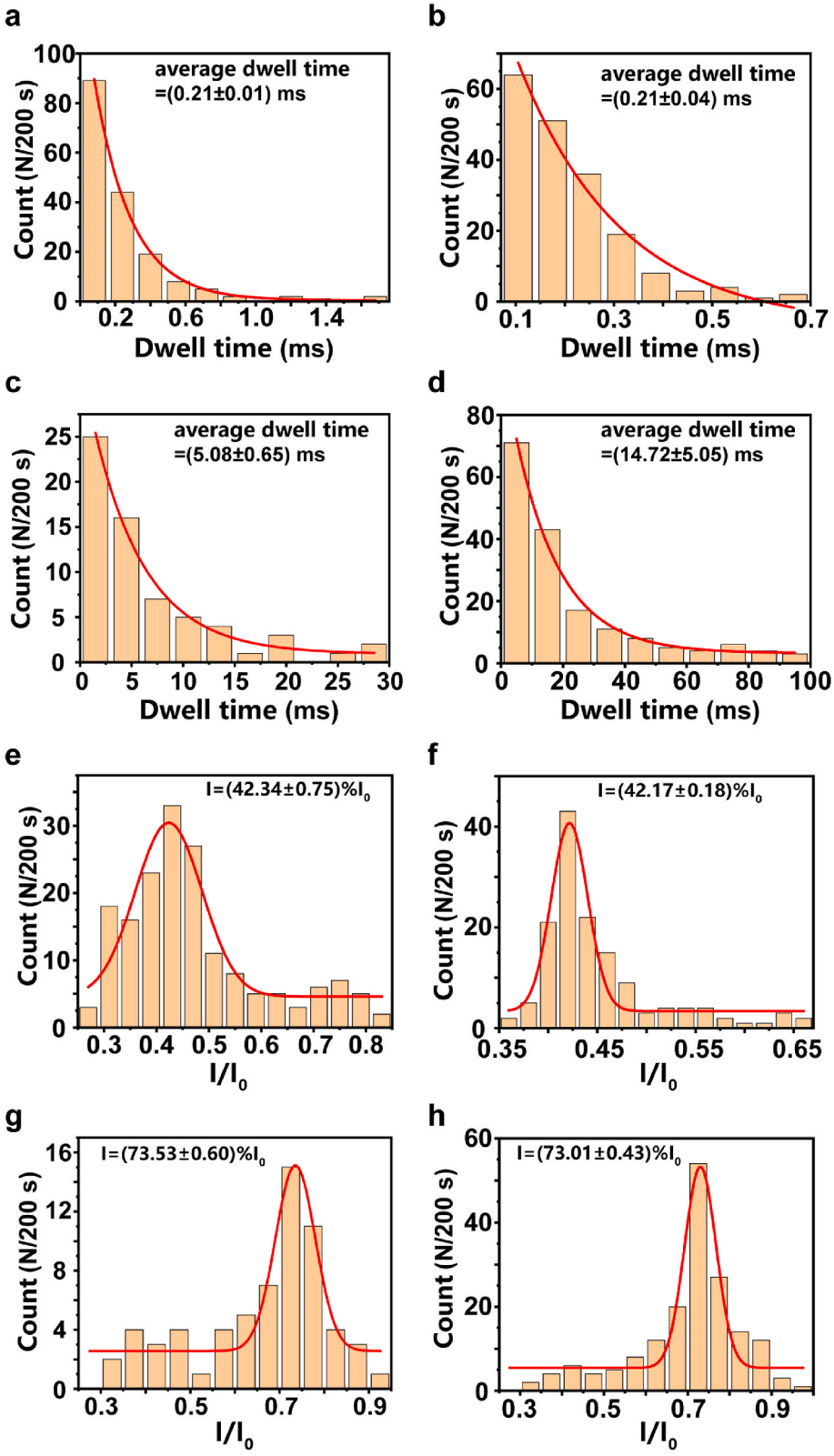

Fig. 3. Statistical analysis of the current blockage signals. (a–d) Dwell time histograms of the current blockage signals of magnetic beads supernatant (a), pure probe ssDNA (b), magnetic beads supernatant using $CaCl_2$ buffer (c), and magnetic beads supernatant using NaCl buffer (d). The solid lines are the single exponential fit to the histograms. (e–h) Amplitude histograms of the current blockage signals of magnetic beads supernatant (e), pure probe ssDNA (f), magnetic beads supernatant using $CaCl_2$ buffer (g), and magnetic beads supernatant using NaCl buffer (h). The solid lines are the Gaussian fit to the histograms.

immobilization. The dsDNA-magnetic beads were washed three times, and then the binding buffer solution with OTA (final concentration of 2 μmol/L) was added [32]. After 2 h incubation, the supernatant was added into the *trans* chamber (10 mmol/L Tris-HCl, 1.0 mol/L NaCl, pH 8) of nanopore detection cell. When a negative voltage (−160 mV) was applied in *trans* chamber, the current traces of α-HL nanopore was recorded. Many current blockage signals occurred with a frequency of 174 N/200 s, and their characteristics were analyzed (Fig. 2a). Fig. 2c showed the signal shape of the probe ssDNA as it passes through the nanopore. To verify the origin of these signals, we performed the control experiment. When solution without OTA was incubated with dsDNA-magnetic beads and added into *trans* chamber of nanopore, rare

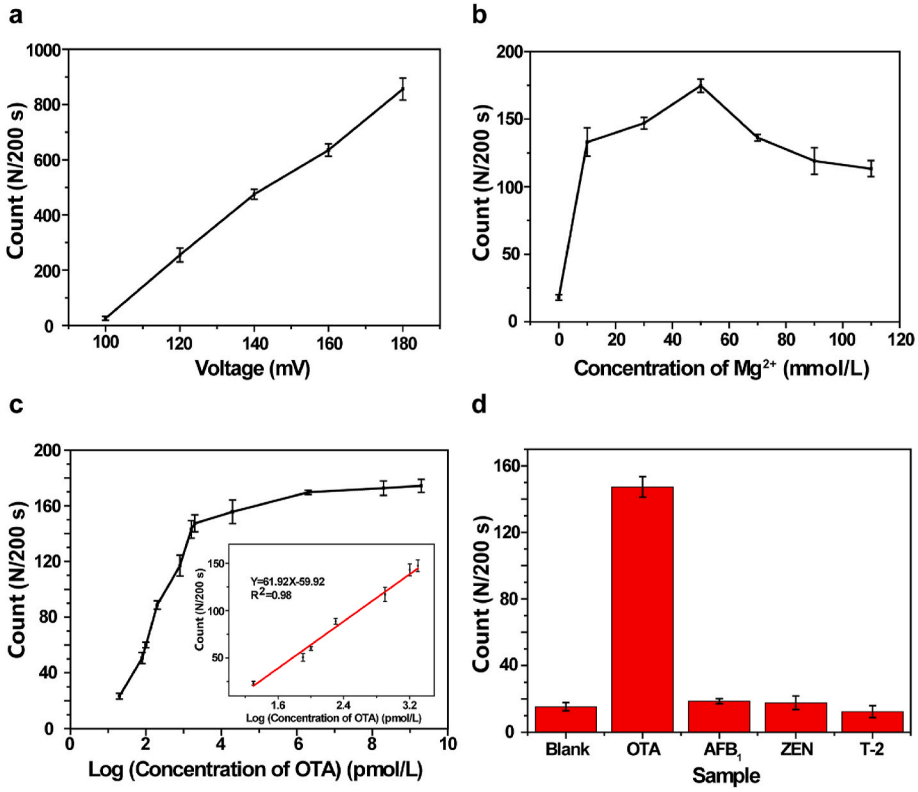

Fig. 4. The optimization of detection conditions and the performance of the aptamer-assisted nanopore sensor. (a) The relationship between signal numbers of probe ssDNA and voltage. (b) The effect of Mg^{2+} concentration in the binding buffer on the signal number of the probe ssDNA. (c) The relationship between the number of probe ssDNA and different concentrations of OTA: 20, 80, 100, 200, 800, 1600, 2000, 2×10^4, 2×10^6, 2×10^8, 2×10^9 pmol/L. The inset showed the linear relationship between the number of probe ssDNA signals and the logarithmic value of the OTA concentration. Experimental conditions: the electrolytic buffer was 1 mol/L NaCl, 10 mmol/L Tris-HCl, pH 8; the binding buffer solution was 1.2 mol/L NaCl, 50 mmol/L KCl, 50 mmol/L $MgCl_2$, 10 mmol/L Tris, pH 8.5; all experiments were performed at the voltage of −160mV. Each data point was the average of three measurements, and the error bar was the standard deviation (n = 3). (d) Histogram of selectivity in the presence of 200 pmol/L fungal toxins: blank, OTA, AFB_1, ZEN, T-2. Three parallel experiments were done for each data point to take the average.

current blockage signal was observed (Fig. 2b). The average dwell time is about 0.21 ± 0.01 ms (Fig. 3a) and residual current ratio (I/I_0) is 0.42 ± 0.01 (Fig. 3e). In addition, pure probe ssDNA (final concentration of 800 nmol/L) was solely added in *trans* chamber. The characteristics of current blockage signals for probe ssDNA (dwell time, I/I_0) were almost the same as those of magnetic beads supernatant (Fig. 3b and f). Consequently, OTA can bind with the aptamers of dsDNA-magnetic beads to release probe ssDNA, which can cause current blockage in the nanopore.

To improve the performance of the OTA nanopore sensor, several factors were optimized. The sequence of probe ssDNA comprised 10 nt probe ssDNA and poly $(dC)_{10}$ tag in the 5' end. As shown in Fig. 2d and e, the poly $(dC)_{10}$ tag greatly improved the signal frequency (37 N/200 s without tag vs. 174 N/200 s with tag), which was favorable for quantitative detection of OTA.

As reported in other works, the cation ions in electrolytic buffers have an impact on the translocation process of ssDNA in nanopore. We tested OTA aptamer as a model analyte to investigate the effect of electrolytic buffers on the translocation process of ssDNA in nanopore [33]. Four common buffers were used, i.e., NH_4Cl, KCl, $CaCl_2$, and NaCl. As shown in Figure S5, compared with other electrolytic buffers with the same concentration, NaCl buffer produced the highest signal frequency (134 N/200 s) with a dwell time of 14.72 ± 5.05 ms (Fig. 3d and h). Meanwhile, ssDNA produced prolonged and even irreversible blockage in NH_4Cl and KCl solution. When the nanopore is occupied by one ssDNA molecule, other molecules cannot enter the pore. Therefore, the frequency of current blockages of ssDNA would reduce dramatically. In $CaCl_2$ solution, the dwell time of blockage was short (5.08 ± 0.65 ms) but the frequency was extremely low (17 N/200 s) (Fig. 3c and g). Consequently, NaCl was used as the electrolytic buffer for subsequent experiments.

In the electrolytic buffer of 1 mol/L NaCl, −100, −120, −140, −160, and −180 mV were applied to observe the signal of the probe ssDNA within 40 s, respectively. As shown in Fig. 4a and S6, the signal frequency of the probe ssDNA increased with the increase of voltage. However, when the applied voltage was too high (more than −180 mV), it had a negative impact on the stability of the phospholipid membrane. Therefore, we chose −160 mV as the optimal voltage for subsequent research.

It has been reported that Mg^{2+} or Ca^{2+} plays a particularly important role in the binding process of aptamer and OTA [23]. So, we selected Mg^{2+} as a critical component in the binding buffer in the experiments. It can be seen from Fig. 4b that the signal frequency of probe ssDNA increased with the increase of Mg^{2+} concentration in the range of 0–50 mmol/L. However, the signal frequency of probe ssDNA decreased when the Mg^{2+} concentration exceeded 50 mmol/L. This phenomenon may result from the chelation between probe ssDNA and Mg^{2+}. When Mg^{2+} concentration is high enough, the effective charge of probe ssDNA in solution is shielded, causing a weak electric field force in nanopore [34]. Therefore, we chose 50 mmol/L as the concentration of Mg^{2+} in the binding buffer during the subsequent experiments.

3.5. Performance of aptamer-assisted nanopore sensor

Under the optimal condition, we tested the performance of the aptamer-assisted nanopore sensor for OTA. Current blockage signals with amplitude of more than 30% of the opening current were counted. As shown in Fig. 4c and S7, the signal frequency of ssDNA increased gradually with the increase of OTA concentration in the range of 2×10^1–2×10^9 pmol/L. In the range of 2×10^1–2×10^3 pmol/L, the logarithm value of OTA concentration has a good linear relationship with the number of ssDNA probe signals. The linear regression equation is $Y = 61.92X - 59.92$, and the correlation coefficient is $R^2 = 0.98$, where Y is the signal number of the probe ssDNA and X was the concentration of OTA. The limit of detection (LOD) is the lowest OTA concentration needed to produce a signal greater than 3 times the standard deviation (3σ) of the noise level (S/N = 3). The LOD calculated in this experiment is about 1.697 pmol/L which confirms that the designed aptamer-assisted nanopore sensor could accomplish the efficient and ultrasensitive detection for OTA. By comparing the performance of the aptamer-

Table 1
Comparison of various methods for OTA sensing.

Method	Detection strategy	Linear range	LOD	Reference
Chemiluminescence	Chemiluminescence resonance energy transfer (CRET) aptasensor	0.1–100 ng/mL (0.248–247.641 nmol/L)	0.22 ng/mL (0.545 nmol/L)	[35]
Fluorescence	Aptamer structure switch with ZnPPIX probe	0.1–1.2 nmol/L	0.03 nmol/L	[36]
Electrochemical	A screen-printed carbon electrode (SPCE) modified with polythionine (PTH) and iridium oxide nanoparticles (IrO_2 NPs)	0.01–100 nmol/L	0.014 nmol/L	[37]
Colorimetric	DNA amplification (Hybridization chain reaction)	0.01–3.2 nmol/L	0.01 nmol/L	[38]
Chemiluminescence	Signal amplified strategy based on target-induced strand release coupling cleavage of nicking endonuclease	1.0×10^{-12}–1.0×10^{-10} g/mL (0.002–0.248 nmol/L)	3.0×10^{-13} g/mL (742.924 fmol/L)	[39]
Electrochemiluminescence	Loop-mediated isothermal amplification (LAMP) technique	0.00005–100 nmol/L	10 fmol/L	[40]
Single-molecule techniqu	Immobilized-aptamer based nanopore sensor	2×10^{1}–2×10^{3} pmol/L	1.698 pmol/L	This work

assisted nanopore sensor with other methods reported in the literature, it can be seen that this method has a very low detection limit (Table 1). In order to study the selectivity of the sensor, other toxins, including Aflatoxin B_1 (AFB_1), ZEN and T-2, were also investigated (Fig. 4d). The developed aptamer-assisted nanopore sensor showed a high affinity for OTA and a low response to other toxins.

To evaluate the reliability of the aptamer-assisted nanopore sensor, real samples were tested. Three known concentrations of OTA (0.2, 0.5, 1 nmol/L) were added to the corn samples, and the aptamer-assisted nanopore sensor was used to detect OTA (Table S1). OTA recoveries were calculated according to the signal frequencies and standard curves ($Y = 61.92X\text{-}59.92$). The calculated recoveries were 109.17%, 95.20% and 97.13%, and relative standard deviation (RSD) were ±7.10, ±4.54, ±2.42, respectively. The result above indicated that the prepared aptamer-assisted nanopore sensor had acceptable accuracy for the detection of OTA in real samples.

4. Conclusion

An immobilized aptamer-based signal conversion strategy has been adopted to detect small molecules (ochratoxin A, OTA) by the nanopore technique. OTA could bind to the aptamer and release probe ssDNA, which could subsequently cause current blockage in the α-HL nanopore. An integrated nanopore current amplifier has been designed and constructed, showing a high performance in noise level and bandwidth. Based on our novel sensing strategy and customizable instrument, we have achieved the ultra-sensitive detection of OTA in corn samples. Our sensing strategy has reached a detection limit of OTA as low as 1.697 pmol/L, which may be the best performance among OTA detection methods. This strategy will broaden the applicability of the nanopore technique and has the potential for rapid and *in-situ* detection of other food contaminants in the future.

Credit author statement

Tong Li: Conceptualization, Writing – original draft preparation; Zhuoqun Su: Methodology, Formal analysis, manuscript editing; Yanan Li: Results discussion; Lingyi Xi: Formal analysis; Guoliang Li: Supervision, Methodology, Writing - reviewing and editing.

Declaration of competing interest

The authors declare that they have no known competing financial interests or personal relationships that could have appeared to influence the work reported in this paper.

Acknowledgments

This work was supported by the National Natural Science Foundation of China (32022069 and 22076115) and the Youth Innovation Team of Shaanxi Universities (21JP020).

Appendix A. Supplementary data

Supplementary data to this article can be found online at https://doi.org/10.1016/j.talanta.2022.123619.

References

[1] E. Macchia, K. Manoli, B. Holzer, C. Di Franco, M. Ghittorelli, F. Torricelli, D. Alberga, G.F. Mangiatordi, G. Palazzo, G. Scamarcio, L. Torsi, Single-molecule detection with a millimetre-sized transistor, Nat. Commun. 9 (2018) 1–10, https://doi.org/10.1038/s41467-018-05235-z.
[2] E. Macchia, K. Manoli, C. Di Franco, G. Scamarcio, L. Torsi, New trends in single-molecule bioanalytical detection, Anal. Bioanal. Chem. 412 (2020) 5005–5014, https://doi.org/10.1007/s00216-020-02540-9.
[3] R. Alexander Reese, B. Xu, Single-molecule detection of proteins and toxins in food using atomic force microscopy, Trends Food Sci. Technol. 87 (2019) 26–34, https://doi.org/10.1016/j.tifs.2019.03.031.
[4] Z. Su, T. Li, D. Wu, Y. Wu, G. Li, Recent progress on single-molecule detection technologies for food safety, J. Agric. Food Chem. 70 (2022) 458–469, https://doi.org/10.1021/acs.jafc.1c06808.
[5] Z. Su, T. Li, G. Li, Application of nanopore-based single molecule detection technology in food safety, Fut. Food Sci. 1 (2021) 44, https://doi.org/10.12281/ffs2708-1893-20210909-004.
[6] F. Yao, X. Peng, Z. Su, L. Tian, Y. Guo, X. Kang, Crowding-Induced DNA translocation through a protein nanopore, Anal. Chem. 92 (2020) 3827–3833, https://doi.org/10.1021/acs.analchem.9b05249.
[7] Y. Long, J.J. Gooding, Nanopores for sensing, ACS Sens. 3 (2018) 2471–2472, https://doi.org/10.1021/acssensors.8b01501.
[8] X.-Q. Ran, H.-L. Qian, X.-P. Yan, Aptamer self-assembly-functionalized nanochannels for sensitive and precise detection of chloramphenicol, Anal. Chem. 93 (2021) 14287–14292, https://doi.org/10.1021/acs.analchem.1c03396.
[9] A. Fragasso, S. Schmid, C. Dekker, Comparing current noise in biological and solid-state nanopores, ACS Nano 14 (2020) 1338–1349, https://doi.org/10.1021/acsnano.9b09353.
[10] Z.-L. Hu, M.-Z. Huo, Y.-L. Ying, Y.-T. Long, Biological nanopore approach for single-molecule protein sequencing, Angew. Chem. Int. Ed. 60 (2021) 14738–14749, https://doi.org/10.1002/anie.202013462.
[11] L. Liu, H.-C. Wu, DNA-based nanopore sensing, Angew. Chem. Int. Ed. 55 (2016) 15216–15222, https://doi.org/10.1002/anie.201604405.
[12] Y.-D. Yin, L. Zhang, X.-Z. Leng, Z.-Y. Gu, Harnessing biological nanopore technology to track chemical changes, TrAC Trends Anal. Chem. (Reference Ed.) 133 (2020) 116091, https://doi.org/10.1016/j.trac.2020.116091.
[13] A. Nehra, S. Ahlawat, K.P. Singh, A biosensing expedition of nanopore: a review, Sensor. Actuator. B Chem. 284 (2019) 595–622, https://doi.org/10.1016/j.snb.2018.12.143.
[14] D. Rotem, L. Jayasinghe, M. Salichou, H. Bayley, Protein detection by nanopores equipped with aptamers, J. Am. Chem. Soc. 134 (2012) 2781–2787, https://doi.org/10.1021/ja2105653.
[15] H. Sun, F. Yao, Z. Su, X.-F. Kang, Hybridization chain reaction (HCR) for amplifying nanopore signals, Biosens. Bioelectron. 150 (2020) 111906, https://doi.org/10.1016/j.bios.2019.111906.
[16] Z. Su, Y. Wei, X. Kang, Simultaneous high-resolution detection of bioenergetic molecules using biomimetic-receptor nanopore, Anal. Chem. 91 (2019) 15255–15259, https://doi.org/10.1021/acs.analchem.9b04268.
[17] G. Sivaraman, R.G. Amorim, R.H. Scheicher, M. Fyta, Benchmark investigation of diamondoid-functionalized electrodes for nanopore DNA sequencing, Nanotechnology 27 (2016) 414002, https://doi.org/10.1088/0957-4484/27/41/414002.
[18] S. Zhuo, Y. Wang, X.-F. Kang, Engineered protein nanopore for real-time monitoring single-molecule reaction between cadmium ion and glutathione, Chin. J. Anal. Chem. 45 (2017) 1172–1178, https://doi.org/10.1016/S1872-2040(17)61032-6.
[19] M. Boukhet, N.F. König, A.A. Ouahabi, G. Baaken, J.-F. Lutz, J.C. Behrends, Translocation of precision polymers through biological nanopores, Macromol. Rapid Commun. 38 (2017) 1700680, https://doi.org/10.1002/marc.201700680.

[20] L. Wang, X. Chen, S. Zhou, G.M. Roozbahani, Y. Zhang, D. Wang, X. Guan, Displacement chemistry-based nanopore analysis of nucleic acids in complicated matrices, Chem. Commun. 54 (2018) 13977–13980, https://doi.org/10.1039/C8CC07944G.
[21] Y. Han, S. Zhou, L. Wang, X. Guan, Nanopore back titration analysis of dipicolinic acid, Electrophoresis 36 (2015) 467–470, https://doi.org/10.1002/elps.201400255.
[22] L. Liu, T. Li, S. Zhang, P. Song, B. Guo, Y. Zhao, H.-C. Wu, Simultaneous quantification of multiple cancer biomarkers in blood samples through DNA-assisted nanopore sensing, Angew. Chem. Int. Ed. 57 (2018) 11882–11887, https://doi.org/10.1002/anie.201803324.
[23] J.A. Cruz-Aguado, G. Penner, Determination of ochratoxin A with a DNA aptamer, J. Agric. Food Chem. 56 (2008) 10456–10461, https://doi.org/10.1021/jf801957h.
[24] T. Li, L. Liu, Y. Li, J. Xie, H.-C. Wu, A universal strategy for aptamer-based nanopore sensing through host–guest interactions inside α-hemolysin, Angew. Chem. 127 (2015) 7678–7681, https://doi.org/10.1002/ange.201502047.
[25] J.G. Bruno, A.M. Richarte, Development and characterization of an enzyme-linked DNA aptamer-magnetic bead-based assay for human IGF-I in serum, Microchem. J. 124 (2016) 90–95, https://doi.org/10.1016/j.microc.2015.08.002.
[26] J.G. Bruno, A.M. Richarte, T. Phillips, A.A. Savage, J.C. Sivils, A. Greis, M. W. Mayo, Development of a fluorescent enzyme-linked DNA aptamer-magnetic bead sandwich assay and portable fluorometer for sensitive and rapid Leishmania detection in sandflies, J. Fluoresc. 24 (2014) 267–277, https://doi.org/10.1007/s10895-013-1315-6.
[27] Y. Wang, Y. Zhang, X. Chen, X. Guan, L. Wang, Analysis with biological nanopore: on-pore, off-pore strategies and application in biological fluids, Talanta 223 (2021) 121684, https://doi.org/10.1016/j.talanta.2020.121684.
[28] P. Jonas, M.E. Bräu, M. Hermsteiner, W. Vogel, Single-channel recording in myelinated nerve fibers reveals one type of Na channel but different K channels, Proc. Natl. Acad. Sci. Unit. States Am. 86 (1989) 7238–7242, https://doi.org/10.1073/pnas.86.18.7238.
[29] Z. Gu, H. Wang, Y.-L. Ying, Y.-T. Long, Ultra-low noise measurements of nanopore-based single molecular detection, Sci. Bull. 62 (2017) 1245–1250, https://doi.org/10.1016/j.scib.2017.09.005.
[30] V. Shlyonsky, D. Gall, The OpenPicoAmp-100k: an open-source high-performance amplifier for single channel recording in planar lipid bilayers, Pflueg. Arch. Eur. J. Physiol. 471 (2019) 1467–1480, https://doi.org/10.1007/s00424-019-02319-7.
[31] A. Bahreyni, H. Luo, M. Ramezani, M. Alibolandi, V. Soheili, N.M. Danesh, M. S. Ashjaei, K. Abnous, S.M. Taghdisi, A fluorescent sensing strategy for ultrasensitive detection of oxytetracycline in milk based on aptamer-magnetic bead conjugate, complementary strand of aptamer and PicoGreen, Spectrochim. Acta. A. Mol. Biomol. Spectrosc. 246 (2021) 119009, https://doi.org/10.1016/j.saa.2020.119009.
[32] Q. Zhao, X.-F. Li, X.C. Le, Aptamer capturing of enzymes on magnetic beads to enhance assay specificity and sensitivity, Anal. Chem. 83 (2011) 9234–9236, https://doi.org/10.1021/ac203063z.
[33] J.W. Shim, Q. Tan, L.-Q. Gu, Single-molecule detection of folding and unfolding of the G-quadruplex aptamer in a nanopore nanocavity, Nucleic Acids Res. 37 (2009) 972–982, https://doi.org/10.1093/nar/gkn968.
[34] S. Wang, Y. Wang, S. Yan, X. Du, P. Zhang, H.-Y. Chen, S. Huang, Retarded translocation of nucleic acids through α-hemolysin nanopore in the presence of a calcium flux, ACS Appl. Mater. Interfaces 12 (2020) 26926–26935, https://doi.org/10.1021/acsami.0c05626.
[35] E.-J. Jo, H. Mun, S.-J. Kim, W.-B. Shim, M.-G. Kim, Detection of ochratoxin A (OTA) in coffee using chemiluminescence resonance energy transfer (CRET) aptasensor, Food Chem. 194 (2016) 1102–1107, https://doi.org/10.1016/j.foodchem.2015.07.152.
[36] F. Liu, A. Ding, J. Zheng, J. Chen, B. Wang, A label-free aptasensor for ochratoxin a detection based on the structure switch of aptamer, Sensors 18 (2018) 1769, https://doi.org/10.3390/s18061769.
[37] L. Rivas, C.C. Mayorga-Martinez, D. Quesada-González, A. Zamora-Gálvez, A. de la Escosura-Muñiz, A. Merkoçi, Label-free impedimetric aptasensor for ochratoxin-A detection using iridium oxide nanoparticles, Anal. Chem. 87 (2015) 5167–5172, https://doi.org/10.1021/acs.analchem.5b00890.
[38] C. Wang, X. Dong, Q. Liu, K. Wang, Label-free colorimetric aptasensor for sensitive detection of ochratoxin A utilizing hybridization chain reaction, Anal. Chim. Acta 860 (2015) 83–88, https://doi.org/10.1016/j.aca.2014.12.031.
[39] X. Hun, F. Liu, Z. Mei, L. Ma, Z. Wang, X. Luo, Signal amplified strategy based on target-induced strand release coupling cleavage of nicking endonuclease for the ultrasensitive detection of ochratoxin A, Biosens. Bioelectron. 39 (2013) 145–151, https://doi.org/10.1016/j.bios.2012.07.005.
[40] Y. Yuan, S. Wei, G. Liu, S. Xie, Y. Chai, R. Yuan, Ultrasensitive electrochemiluminescent aptasensor for ochratoxin A detection with the loop-mediated isothermal amplification, Anal. Chim. Acta 811 (2014) 70–75, https://doi.org/10.1016/j.aca.2013.11.022.